

A PAC-Bayesian bound for deterministic classifiers

Eugenio Clerico

Department of Statistics, University of Oxford

CLERICO@STATS.OX.AC.UK

George Deligiannidis

Department of Statistics, University of Oxford

DELIGIAN@STATS.OX.AC.UK

Benjamin Guedj

Centre for Artificial Intelligence and Department of Computer Science, University College London & Inria London

B.GUEDJ@UCL.AC.UK

Arnaud Doucet

Department of Statistics, University of Oxford

DOUCET@STATS.OX.AC.UK

Abstract

We establish a disintegrated PAC-Bayesian bound for classifiers that are trained via continuous-time (non-stochastic) gradient descent. Contrarily to what is standard in the PAC-Bayesian setting, our result applies to a training algorithm that is deterministic, conditioned on a random initialisation, without requiring any *de-randomisation* step. We provide a broad discussion of the main features of the bound that we propose, and we study analytically and empirically its behaviour on linear models, finding promising results.

1. Introduction

Effectively upper-bounding the generalisation error of modern learning algorithms is a major open challenge for the statistical learning theory community (Zhang et al., 2016). Originally, properties of the hypothesis space, such as VC dimension and Rademacher complexity (Vapnik, 2000; Bousquet et al., 2004; Shalev-Shwartz and Ben-David, 2014), were used to establish *worst-case* generalisation bounds, holding uniformly over all possible algorithms and training datasets. However, as these results are often vacuous for the current over-parameterised models, the modern perspective focuses on algorithm- and data-dependent bounds (McAllester, 1998; Bousquet and Elisseeff, 2002; Dwork and Roth, 2014; Hardt et al., 2016; Xu and Raginsky, 2017; Clerico et al., 2022b; Lugosi and Neu, 2022). Among the various approaches, the PAC-Bayesian framework (Guedj, 2019; Alquier, 2021) has obtained promising empirical results for deep networks (Dziugaite and Roy, 2017; Zhou et al., 2019; Pérez-Ortiz et al., 2021a,b; Biggs and Guedj, 2022b; Clerico et al., 2022a).

Typically, a PAC-Bayesian bound is an upper bound on the expected population loss of a stochastic classifier, holding with high probability on the random draw of the training dataset. This setting, with intrinsically random model parameters, does not match with the standard scenario of a non-randomised predictor. Although most available empirical PAC-Bayesian studies on neural networks focus on specifically designed stochastic architectures (Dziugaite and Roy, 2017; Zhou et al., 2019; Pérez-Ortiz et al., 2021a; Clerico et al., 2022a), there are also *de-randomisation* methods allowing to apply PAC-Bayesian ideas to deterministic classifiers. For instance, under suitable stability assumptions, one upper-bounds the generalisation of a deterministic model via a PAC-Bayesian analysis of a noisy version of it, with stochastically perturbed parameters (Neysshabur et al., 2018; Nagarajan and Kolter, 2019; Miyaguchi, 2019). Alternatively, averaging a stochastic

algorithm yields a deterministic one, and one can obtain PAC-Bayesian bounds on the loss of this averaged predictor via Jensen’s inequality (if the loss function is convex) (Germain et al., 2009; Letarte et al., 2019; Biggs and Guedj, 2021) or margin-based arguments (Langford and Shawe-Taylor, 2002; Banerjee et al., 2020; Biggs and Guedj, 2022a). Finally, besides the PAC-Bayesian bounds in expectation, there are disintegrated results that hold with high probability on a random realisation of the stochastic algorithm (Catoni, 2004, 2007; Blanchard and Fleuret, 2007; Alquier and Biau, 2013; Guedj and Alquier, 2013; Rivasplata et al., 2020; Viillard et al., 2021). In the case of a stochastic network, this means that we can get a generalisation bound for the deterministic classifier obtained by drawing all the parameters once.

When trying to apply the PAC-Bayesian framework to study a given non-stochastic model, the first of the methods above is the most natural. However, in the present work, we show that for this purpose it is also possible to leverage disintegrated PAC-Bayesian bounds. Our starting point is noticing that even training a *deterministic* classifier does usually involve some randomness: the standard procedure when training a neural network almost always starts with the random draw of the initial weights (Goodfellow et al., 2016). For a model trained via continuous-time (non-stochastic) gradient descent, we show that it is possible to exploit this source of stochasticity and obtain a disintegrated PAC-Bayes bound that holds with high probability on the random training dataset and initialisation (Proposition 3). Evaluating this bound only requires to know the density for the initial and final configurations of the network, and to compute the integral of the training objective’s Laplacian along the trajectory. Although the bound necessitates the *ideal* situation of continuous training dynamics, to our knowledge this is the first PAC-Bayesian result that directly applies to a general standard non-stochastic neural network with a deterministic gradient descent training, without strong assumptions on the architecture or the need of any auxiliary stochastic model. Besides, our bound is remarkably easy-to-prove and simple, with no restrictive hypothesis made on the training objective, which is only required to be twice differentiable.

Although our bound does not hold for non-continuous training dynamics, a disintegrated PAC-Bayesian result can still be established by replacing the gradient descent optimisation with suitably discretised damped Hamiltonian dynamics. However, a few empirical results seem to suggest that the bounds obtained in this way may actually be much looser than those yielded by the gradient flow dynamics. For the sake of conciseness, in the present paper we only quickly outline this Hamiltonian approach, deferring a more thorough analysis to future work.

2. Notation and setting

In a standard supervised learning framework, we consider pairs $(x, y) \in \mathcal{X} \times \mathcal{Y}$, where x denotes an example and y its label. We assume that there is a mapping $f^* : \mathcal{X} \rightarrow \mathcal{Y}$ that associates to each x a unique correct label $y = f^*(x)$. A learning algorithm takes a training dataset $s = \{x_1 \dots x_m\}$ of m inputs whose labels $\{f^*(x_1) \dots f^*(x_m)\}$ are known, and outputs a function $f : \mathcal{X} \rightarrow \mathcal{Y}$, ideally a good approximation of f^* . More generally, the algorithm will return a hypothesis $h \in \mathcal{H}$ (e.g., values of a neural network’s parameters), which is understood to parameterise a map $f_h : \mathcal{X} \rightarrow \mathcal{Y}$. We will always assume that $\mathcal{H} = \mathbb{R}^N$, for some dimension $N > 0$. We call the algorithm stochastic when its output h is a random variable on \mathcal{H} , whose law can depend on s .

The performance of each hypothesis can be assessed via a loss function ℓ , which takes a pair of labels (y, y') and returns a real value, representing how “far apart” y and y' are. In practice, for any

hypothesis h , one can always compute the empirical loss on the training dataset

$$\mathcal{L}_s(h) = \frac{1}{m} \sum_{x \in s} \ell(f_h(x), f^*(x)).$$

However, what often matters is how well h predicts the labels of instances x not belonging to s . Assuming that the population of examples follows a distribution μ , the relevant quantity is the population loss

$$\mathcal{L}_{\mathcal{X}}(h) = \int_{\mathcal{X}} \ell(f_h(x), f^*(x)) d\mu(x).$$

Upper-bounding $\mathcal{L}_{\mathcal{X}}$, having access to \mathcal{L}_s only, is usually referred to as the generalisation problem. Typically, the training dataset is made of m i.i.d. samples from μ (i.e., $s \sim \mu^m = \mu^{\otimes m}$). We are interested in upper bounds on $\mathcal{L}_{\mathcal{X}}(h)$ (where h is the hypothesis picked by the algorithm) that hold with high probability on the random draw of s (or of (h, s) in the stochastic setting).

We mainly focus on algorithms whose output is obtained optimising an objective $\mathcal{C}_s : \mathcal{H} \rightarrow \mathbb{R}$ via continuous-time gradient descent. Clearly, \mathcal{C}_s depends on the training dataset s and, in practice, it can coincide with the empirical loss, although this is not necessarily the case, as one might use a surrogate loss for the training or add some regularisation term. We require the objective to be twice differentiable, and we define the gradient flow $(h_0, t) \mapsto \Phi_t(h_0)$ as the solution of the dynamics

$$\partial_t \Phi_t(h_0) = -\nabla \mathcal{C}_s(\Phi_t(h_0)); \quad \Phi_0(h_0) = h_0. \quad (1)$$

As h_0 is fixed before starting the training, we will often omit the explicit dependence on it, and simply write the solution of (1) as h_t . Fixing a time horizon $T > 0$, the algorithm's output is h_T .

We will consider a random initialisation with law ρ_0 , and define the distribution ρ_t as

$$\rho_t = \Phi_t^\# \rho_0,$$

the push-forward of ρ_0 under the gradient flow. In this way, if we draw h_0 from ρ_0 , then we automatically get that $h_t \sim \rho_t$. Note that h_t is non-random when conditioned on the initialisation h_0 . In particular, although the algorithm is in fact stochastic, we can see it as a *deterministic* model that has only a random initialisation. This is actually the common setting for modern neural networks, whose initial configuration is usually drawn from some simple distribution (e.g., He et al., 2015).

3. Disintegrated PAC-Bayes bounds

The main research focus in the development of the PAC-Bayesian theory has been on bounds in expectation, and only recently Rivasplata et al. (2020) and Viillard et al. (2021) have brought back interest in the disintegrated bounds, which actually date back to the works of Catoni (2004, 2007) and Blanchard and Fleuret (2007). We refer to Alquier (2021) for a detailed introductory exposition of the PAC-Bayesian framework that also discusses a few disintegrated results.

We consider a stochastic model that, given $s \sim \mu^m$, returns a random hypothesis $h \sim \rho^s$, where the superscript s used in this section stresses explicitly ρ 's dependence on s .¹ We denote the joint law of (s, h) as $\mu^m * \rho^s$, that is $d(\mu^m * \rho^s)(s, h) = d\mu^m(s) d\rho^s(h)$. As standard in the PAC-Bayesian literature, we call ρ^s the *posterior* distribution. We let π be a *prior* distribution on \mathcal{H} , whose only

1. To be rigorous, one should actually require that $s \mapsto \rho^s$ is a Markov kernel.

requirement is to be data-agnostic, namely it cannot depend on the specific dataset s used for the training. We write $\mu^m \otimes \pi$ for the law of a pair (s, h) , where $s \sim \mu^m$ and $h \sim \pi$ are independent.

A disintegrated PAC-Bayesian bound is an upper bound on $\mathcal{L}_{\mathcal{X}}(h)$, where h is the output of a stochastic algorithm, that holds with high probability over $(s, h) \sim \mu^m * \rho^s$. The next result, from [Rivasplata et al. \(2020\)](#), allows us to derive several of these bounds.

Proposition 1 *Let $\Psi : \mathbb{R}^2 \rightarrow \mathbb{R}$ be an arbitrary measurable function, and let ξ be the expectation of $e^{\Psi(\mathcal{L}_s(h), \mathcal{L}_{\mathcal{X}}(h))}$ under $(s, h) \sim \mu^m \otimes \pi$. For any $\delta \in (0, 1)$, for any posterior distribution ρ^s absolutely continuous with respect to π , with probability at least $1 - \delta$ on $(s, h) \sim \mu^m * \rho^s$ we have that*

$$\Psi(\mathcal{L}_s(h), \mathcal{L}_{\mathcal{X}}(h)) \leq \log \frac{d\rho^s}{d\pi}(h) + \log \frac{\xi}{\delta}.$$

Proof By Markov's inequality, for $(s, h) \sim \mu^m * \rho^s$ we have that with probability at least $1 - \delta$

$$e^{\Psi(\mathcal{L}_s(h), \mathcal{L}_{\mathcal{X}}(h)) - \log \frac{d\rho^s}{d\pi}(h)} \leq \frac{1}{\delta} \int_{\mathcal{X}^m \times \mathcal{H}} e^{\Psi(\mathcal{L}_s(h), \mathcal{L}_{\mathcal{X}}(h)) - \log \frac{d\rho^s}{d\pi}(h)} d\mu^m(s) d\rho^s(h).$$

As $\int_{\mathcal{H}} e^{\Psi(\mathcal{L}_s(h), \mathcal{L}_{\mathcal{X}}(h)) - \log \frac{d\rho^s}{d\pi}(h)} d\rho^s(h) = \int_{\mathcal{H}} e^{\Psi(\mathcal{L}_s(h), \mathcal{L}_{\mathcal{X}}(h))} d\pi(h)$, $\forall s \in \mathcal{X}^m$, we conclude. \blacksquare

Choosing $\Psi(u, v) = 2m(u - v)^2$ one finds the disintegrated version of a standard PAC-Bayesian bound by [McAllester \(1999\)](#). Alternatively, defining $\text{kl}(u||v) = u \log \frac{u}{v} + (1 - u) \log \frac{1-u}{1-v}$ (the relative entropy between two binary Bernoulli distributions) and setting $\Psi(u, v) = m \text{kl}(u||v)$, we get a tighter bound, which is the disintegrated counterpart of a bound due to [Langford and Seeger \(2001\)](#) and [Maurer \(2004\)](#). These results follow from the fact that in both cases ξ can be upper-bounded by $2\sqrt{m}$, if the loss ℓ is bounded in $[0, 1]$ ([Bégin et al., 2016](#)).

Corollary 2 *Assume that the loss ℓ is bounded in $[0, 1]$. For any $\delta \in (0, 1)$, for any posterior distribution ρ^s absolutely continuous with respect to π , each of the bounds below (where $\text{kl}^{-1}(u|c) = \sup\{v \in [0, 1] : \text{kl}(u||v) \leq c\}$) holds with probability at least $1 - \delta$ on $(s, h) \sim \mu^m * \rho^s$:*

$$\begin{aligned} \mathcal{L}_{\mathcal{X}}(h) &\leq \mathcal{L}_s(h) + \sqrt{\frac{\log \frac{d\rho^s}{d\pi}(h) + \log \frac{2\sqrt{m}}{\delta}}{2m}}; \\ \mathcal{L}_{\mathcal{X}}(h) &\leq \text{kl}^{-1} \left(\mathcal{L}_s(h) \left| \frac{\log \frac{d\rho^s}{d\pi}(h) + \log \frac{2\sqrt{m}}{\delta}}{m} \right. \right). \end{aligned}$$

4. Disintegrated bounds under gradient flow dynamics

We state here our main result, a disintegrated bound for an algorithm trained by continuous gradient descent optimisation. We recall some notation from Section 2. We let \mathcal{C}_s be a twice differentiable training objective, and we consider a random initialisation $h_0 \sim \rho_0$. The dynamics are described by

$$\partial_t h_t = -\nabla \mathcal{C}_s(h_t),$$

where we omit the explicit dependence of h_t on s and h_0 . The algorithm's output is h_T , for some fixed $T > 0$. We let ρ_t be the push-forward of ρ_0 under the gradient flow, so that $h_t \sim \rho_t$. For all t we assume that ρ_t admits a Lebesgue density, which we write ρ_t , with a slight abuse of notation.

It is natural to choose ρ_0 without relying on the specific dataset s used for the training. In particular, we can select ρ_0 as PAC-Bayesian. On the other hand, ρ_T depends on s through the objective \mathcal{C}_s , and plays the role of posterior. Sampling the model's initialisation h_0 from ρ_0 and following the flow dynamics up to T , we get a hypothesis h_T that is a sample from ρ_T . Thus, saying that an event holds with probability at least $1 - \delta$ under $(s, h_T) \sim \mu^m * \rho_T$ is equivalent to state that it has probability at least $1 - \delta$ under $(s, h_0) \sim \mu^m \otimes \rho_0$. We can hence use Proposition 1 to obtain a PAC-Bayesian generalisation bound for an algorithm that, once drawn s and h_0 , is deterministic.

So far, we have a bound that involves the term $\rho_T(h_T)/\rho_0(h_T)$. Typically, the density ρ_0 is known, and evaluating $\rho_0(h_T)$ does not pose any problem. On the other hand, computing $\rho_T(h_T)$ is less straightforward. However, thanks to the continuity of the dynamics, it is possible to keep track of the evolution of $\rho_t(h_t)$ along the training trajectory via a simple trick, usually referred to as ‘‘instantaneous change of variables’’ in the normalising flow literature (Chen et al., 2018).

Proposition 3 *Consider the dynamics $\partial_t h_t = -\nabla \mathcal{C}_s(h_t)$, with $\mathcal{C}_s : \mathcal{H} \rightarrow \mathbb{R}$ twice differentiable. Let $\Psi : \mathbb{R}^2 \rightarrow \mathbb{R}$ be a measurable function. Fixed $\delta \in (0, 1)$ and $T > 0$,² with probability at least $1 - \delta$ on the random draw $(s, h_0) \sim \mu^m \otimes \rho_0$, we have*

$$\Psi(\mathcal{L}_s(h_T), \mathcal{L}_X(h_T)) \leq \log \frac{\rho_0(h_0)}{\rho_0(h_T)} + \int_0^T \Delta \mathcal{C}_s(h_t) dt + \log \frac{\xi}{\delta},$$

where Δ denotes the Laplacian with respect to h and $\xi = \int_{\mathcal{X}^m \times \mathcal{H}} e^{\Psi(\mathcal{L}_s(h), \mathcal{L}_X(h))} d\mu^m(s) d\rho_0(h)$.

Proof Since sampling (s, h_T) from $\mu^m * \rho_T$ is equivalent to drawing $(s, h_0) \sim \mu^m * \rho_0$ and following the dynamics up to T , Proposition 1 yields that, with probability at least $1 - \delta$ on $(s, h_0) \sim \mu^m \otimes \rho_0$,

$$\Psi(\mathcal{L}_s(h_T), \mathcal{L}_X(h_T)) \leq \log \frac{\rho_T(h_T)}{\rho_0(h_T)} + \log \frac{\xi}{\delta}.$$

The gradient flow's continuity equation states that $\partial_t \rho_t(h) = \nabla \cdot (\rho_t(h) \nabla \mathcal{C}_s(h))$, for all $h \in \mathcal{H}$, so $\partial_t(\rho_t(h_t)^2) = \partial_t \rho_t(h_t) + \nabla \rho_t(h_t) \cdot \partial_t h_t = \rho_t(h_t) \Delta \mathcal{C}_s(h_t)$ and $\int_0^T \Delta \mathcal{C}_s(h_t) dt = \log \frac{\rho_T(h_T)}{\rho_0(h_0)}$. ■

Note that the time horizon T must be chosen a priori, as it cannot depend on the specific s and h_0 used for the training. However, through a classical union bound argument, one can slightly loosen the bound while allowing to select the best T from a finite pool of possible values (see Section 5.2).

Clearly, for $\ell \subseteq [0, 1]$, the choices of Ψ that led to Corollary 2 will again bring explicit bounds. Setting $\Psi(u, v) = 2m(u - v)^2$ and $\Psi(u, v) = m \text{kl}(u|v)$ yields respectively

$$\mathcal{L}_X(h_T) \leq \mathcal{L}_s(h_T) + \sqrt{\frac{\log \frac{\rho_0(h_0)}{\rho_0(h_T)} + \log \frac{2\sqrt{m}}{\delta} + \int_0^T \Delta \mathcal{C}_s(h_t) dt}{2m}}; \quad (2)$$

$$\mathcal{L}_X(h_T) \leq \text{kl}^{-1} \left(\mathcal{L}_s(h_T) \left| \frac{\log \frac{\rho_0(h_0)}{\rho_0(h_T)} + \log \frac{2\sqrt{m}}{\delta} + \int_0^T \Delta \mathcal{C}_s(h_t) dt}{m} \right. \right), \quad (3)$$

each bound holding with probability at least $1 - \delta$ on the random initialisation and training dataset.

2. To be fully rigorous, one should explicitly assume that the solution $t \mapsto h_t$ of the dynamics is well defined on $[0, T]$, for all initial conditions $h_0 \in \mathcal{H}$.

We remark that Proposition 3 holds for time-dependent objectives as well (as long as they do not depend on ρ_t), as the gradient flow’s continuity equation is still valid. Leveraging this, we can specialise the result for training with (potentially randomly selected) batches; see Section 5.5 for further details. Also, an interesting alternative scenario is when the continuous-time dynamics are stochastic. For instance, one might consider the Langevin’s diffusion $dh_t = -\nabla\mathcal{C}_s(h_t) + \sigma dB_t$, where $\sigma > 0$ is a fixed coefficient and B_t a Brownian motion. However, in this case we do not end up anymore with an easily tractable exact expression for $\log \frac{\rho_T(h_T)}{\rho_0(h_0)}$ (see Appendix A).

5. Analysis and discussion

5.1. A few comments on the Laplacian term

An interesting feature of the bound in Proposition 3 is the integral of the Laplacian of the optimisation objective along the training path:

$$\int_0^T \Delta\mathcal{C}_s(h_t)dt. \quad (4)$$

Under the gradient flow dynamics, $\Delta\mathcal{C}_s(h_t)$ is keeping track of how the probability density is locally varying. Indeed, from a PAC-Bayesian perspective, for the bound to be small we need to end up in some point where the posterior density is not too high compared to the initial. If we follow a trajectory characterised by a large Laplacian, we see a sharp increase of the density. Intuitively, we can picture the situation as if we were attracting the nearby paths and bringing further *probability mass* around us. The final ρ_T is likely to be much larger than the initial ρ_0 and lead to a loose bound.

It is worth noting that (4) takes a particularly simple form in the one-dimensional case, as it only depends on the initial and final “velocities”. Indeed, $\partial_t\mathcal{C}'_s(h_t) = \mathcal{C}''_s(h_t)\partial_t h_t = -\mathcal{C}''_s(h_t)\mathcal{C}'_s(h_t)$, with \mathcal{C}'_s and \mathcal{C}''_s denoting the first and second derivatives of \mathcal{C}_s . So, $\mathcal{C}''_s(h_t) = -\partial_t \log |\mathcal{C}'_s(h_t)|$ and

$$\int_0^T \mathcal{C}''_s(h_t)dt = \log \frac{\mathcal{C}'_s(h_0)}{\mathcal{C}'_s(h_T)}. \quad (5)$$

On the other hand, things are not that simple in the multidimensional case, where we can find

$$\int_0^T \Delta\mathcal{C}_s(h_t)dt = \log \frac{\|\nabla\mathcal{C}_s(h_0)\|}{\|\nabla\mathcal{C}_s(h_T)\|} - \int_{h_{[0:T]}} \nabla \cdot \tau(h) \|\delta h\|. \quad (6)$$

Here $\tau(h)$ stands for the unit tangent vector to the trajectory in h , and $\int_{h_{[0:T]}} \dots \|\delta h\|$ denotes the line integral along the path $h_{[0:T]}$. The last term has a clear meaning, as it quantifies how much $h_{[0:T]}$ is attracting the nearby trajectories. We refer to Appendix B for a derivation of (6).

Although we are not aware of any generalisation bound that involves the exact term (4), the Laplacian’s integral might find a natural interpretation through the connection between flatness in the loss landscape and good generalisation. The belief that an algorithm able to find wide local optima of the loss performs well on unseen inputs dates back to Hochreiter and Schmidhuber (1997). Re-popularised by Keskar et al. (2017), this idea has been the object of an intense debate, attracting some criticisms as the definitions of *flatness* are often susceptible to re-parameterisations of the hypothesis space (Dinh et al., 2017; Neyshabur et al., 2017). However, numerous recent works have provided empirical and theoretical support, as well as new insights, to the flat minima argument

(Dziugaite and Roy, 2017; Izmailov et al., 2018; He et al., 2019; Neu et al., 2021). Going back to our setting, if we assume that the objective \mathcal{C}_s coincides with the empirical loss, we clearly see that sharper loss’s local optima correspond to higher values of the Laplacian term. Since approaching a wider minimum usually implies a longer convergence time, one might wonder if our bound can actually benefit from flatness in the loss landscape. However, unless we consider a one-dimensional problem, we easily see that the curvature in the directions orthogonal to the trajectory contributes to the Laplacian’s integral, albeit not affecting the training dynamics. So, we expect that converging towards flatter minima will typically yield a tighter bound, especially for high dimensional settings.

5.2. Role of the time horizon

Most of the standard PAC-Bayesian bounds (in expectation) contain the Kullback-Leibler divergence between the and the posterior. This quantity is infinity if the posterior is a Dirac delta, and this is why these results cannot apply directly to the deterministic setting. Even the disintegrated framework is not exempt from this pathological behaviour, which is reflected by the fact that in Proposition 3 we cannot let the time horizon T be infinite even if h_t converges, as the posterior would be degenerate and typically consist in a sum of Dirac deltas centred on the local optima. Concretely, we can easily check that if an algorithm is converging to a local minimum (where \mathcal{C}_s is approximately quadratic), then (2) will asymptotically go as $\mathcal{L}_{\mathcal{X}}(h) - \mathcal{L}_s(h) \lesssim O(\sqrt{T})$, for large T (see Appendix C). However, this is not the only possible asymptotic behaviour. For instance, we can think of situations where h_t is not converging but diverging. As we will see in Section 7, this is what happens for linear models trained to optimise a linear objective or the cross-entropy.

Although characterising the typical spectrum of the Hessian of the loss during the training evolution is a challenging open problem, recent empirical studies suggest that after an initial phase where the Laplacian can potentially be negative, later stages of the dynamics are characterised by a few dominant positive Hessian’s eigenvalues (Sagun et al., 2018; Ghorbani et al., 2019). As a consequence, in most situations the Laplacian’s integral will soon become monotonically increasing with T . Moreover, we can expect that $\log \frac{\rho_0(h_0)}{\rho_0(h_T)}$ will grow with T as well, since h_0 is likely to lie in a region where the density is high, and the training will typically push h_t farther and farther from it. Overall, in order to achieve non-vacuous bounds, we need to stop the training at a finite time horizon T , which will play the role of a trade-off between how well we can fit the training dataset, and how much we can keep the bound small.

A final remark, already mentioned earlier, is that T must be chosen independently of the dataset s and initial state h_0 used for the training. However, adding a penalty $\log K$ (*i.e.*, replacing the term $\log \frac{\xi}{\delta}$ with $\log \frac{K\xi}{\delta}$) to the bounds of Propositions 1 and 3 allows us to pick the best time horizon among a set $\{T_1 \dots T_K\}$ of K potential candidates. This follows from an elementary union bound argument, as for each T_k we can consider a bound holding with probability at least $1 - \delta/K$.

5.3. Scaling with the dimension of the hypothesis space

When dealing with generalisation bounds, a natural question is how they scale with the dimension N of the hypothesis space. In our case, the answer is not easy, as it is hard to say how the different bound’s components behave. For instance, we can expect the Laplacian to scale linearly with N , as it is the sum of N terms. If $T \sim O(1)$ and the Laplacian’s integral dominates the bound, (2) becomes $O(\sqrt{N/m})$, a typical behaviour. Conversely, if the term $\log \frac{\rho_0(h_0)}{\rho_0(h_T)}$ brings the main contribution, the scaling with N might be more complex and depend on the choice of the density.

Interestingly, the optimal time horizon T can scale with N as well, and empirical results on MNIST show that for a linear model we can have $T \sim O(1/N)$, and hence obtain non-vacuous bounds even in highly over-parameterised regimes (see Figure 1). Intuitively, when N is large, the algorithm can quickly find a hypothesis that fits well the training data and is “close” enough to h_0 to be quickly reached. On the other hand, fewer learnable parameters might need a longer training before attaining low values of the empirical loss. Despite the simple setting of our experiments, we believe that this is a promising result as the bound seems to not suffer much from the *curse of dimensionality*. However, a more detailed empirical and theoretical analysis is needed in order to gauge how well our bound performs with more complex models, such as deep networks.

5.4. Discretised dynamics

One of the main limitations of the present work is that the bound of Proposition 3 requires a continuous-time gradient descent. Except for a few simple settings, where analytic solutions are available, the standard gradient-based optimisation algorithms consider discretised dynamics, whose trajectories are made of jumps and only approximate the continuous flow. Consequently, in order to leverage our results and get rigorous generalisation bounds for the standard gradient descent optimisers, one would need to control the errors introduced by the time discretisation via a careful analysis, beyond the scope of the present work. Nevertheless, we can at least conjecture that, for small enough learning rates, the results obtained via the discretised dynamics are a good approximation of the exact gradient flow solution. In Figure 2, the relative error between the values of the bound (3), obtained from two different time discretisations, stays small throughout the training, suggesting that the discretised results approximate well the actual continuous dynamics.

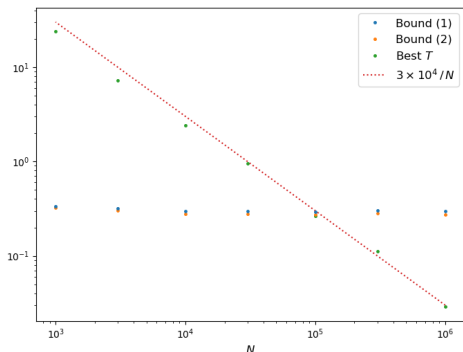


Figure 1: Behaviour of best time horizon T with the model dimension N , from experiments on MNIST for linear models trained to optimise a cross-entropy objective. The optimal T was found to go roughly as $1/N$ (cf. dotted line), preventing the bounds (2) and (3) from exploding, even in highly over-parameterised settings. Note that the results reported here were obtained via discretised gradient dynamics (cf. Section 5.4 and Figure 2). We refer to Appendix F.3 for further details on the experiment.

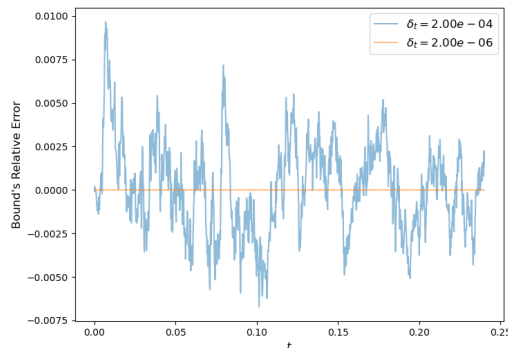


Figure 2: Relative error $(B_1 - B_2)/B_2$, for a linear model with 10^5 parameters trained on MNIST via discretised gradient steps on a cross-entropy objective. Here, B_1 and B_2 are the values of the bound (3) obtained with the time-steps $\delta_{t,1} = 2 \times 10^{-4}$ and $\delta_{t,2} = 2 \times 10^{-6}$ respectively. The small relative error suggests that the corrections to the bound due to the time-discretised dynamics are likely to be negligible. We refer to Appendix F.3 for further details on the experiment.

Interestingly, [Barrett and Dherin \(2021\)](#) remarked that the solutions of the discrete dynamics $h_{k+1} - h_k = -\varepsilon \nabla \mathcal{C}_s(h_k)$ match closely the continuous paths of $\partial_t h_t = -\nabla(\mathcal{C}_s(h_t) + \varepsilon \|\nabla \mathcal{C}_s(h_t)\|^2)$, with an error after a single step of order $O(\varepsilon^3)$ ³. Consequently, if we aim at studying the discrete dynamics, we obtain a more precise approximation of an actual generalisation bound by replacing $\Delta \mathcal{C}_s$ with $\Delta(\mathcal{C}_s(h_t) + \varepsilon \|\nabla \mathcal{C}_s(h_t)\|^2)$. For higher accuracy, one can add further correction terms to \mathcal{C}_s , following standard backward error analysis arguments ([Hairer et al., 2006](#)).

Alternatively, one can consider a different optimisation strategy, which allows to control the evolution of the density ρ_t even for discretised dynamics. As we will discuss in [Section 6](#), this is for instance possible by exploiting the symplectic properties of suitable Hamiltonian integrators.

5.5. Training via batches

So far, we have considered the case of a training objective \mathcal{C}_s that is fixed throughout the training. However, the bound of [Proposition 3](#) also holds for time-dependent objectives. In particular, we can apply our result to the case in which we optimise the empirical loss over different batches of the training dataset. Let us denote as s_1, \dots, s_M the (temporarily ordered) sequence of batches used for the training, where a batch needs to appear multiple times if it is used more than once. It is worth noting that the batches and their order are allowed to be selected randomly, as in the usual stochastic gradient descent optimisation. Then, we can suppose that from $t = 0$ to $t = t_1$ we use \mathcal{C}_{s_1} as optimisation objective, from $t = t_1$ to $t = t_2$ we use \mathcal{C}_{s_2} , and so on until $t_M = T$. We can get a bound as in [Proposition 3](#), with the only difference that $\int_0^T \Delta \mathcal{C}_s(h_t) dt$ is now replaced by

$$\int_0^{t_1} \Delta \mathcal{C}_{s_1}(h_t) dt + \int_{t_1}^{t_2} \Delta \mathcal{C}_{s_2}(h_t) dt + \dots + \int_{t_{M-1}}^{t_M} \Delta \mathcal{C}_{s_M}(h_t) dt. \quad (7)$$

5.6. Data-dependent priors

Most PAC-Bayesian results require the prior to be chosen independently of the dataset used to evaluate the bound. However, we can learn the prior on an additional dataset s' (independent of s), a strategy proposed by [Seeger \(2002\)](#) that has yielded the tightest currently available empirical PAC-Bayesian bounds on MNIST and CIFAR10 ([Pérez-Ortiz et al., 2021a](#); [Clerico et al., 2022a](#)).

In our setting we might proceed in a similar way. Till a fixed time t_0 , we follow the dynamics $\partial_t h_t = -\nabla \mathcal{C}_{s'}(h_t)$, and we select ρ_{t_0} as the PAC-Bayesian prior. Then, we let \mathcal{C}_s be the training objective and we follow the gradient flow from t_0 until the time horizon T . To evaluate the bound, we need to compute $\log \frac{\rho_T(h_T)}{\rho_{t_0}(h_T)}$. Proceeding as in the proof of [Proposition 3](#), we get

$$\log \frac{\rho_T(h_T)}{\rho_{t_0}(h_T)} = \log \frac{\rho_0(h_0)}{\rho_{t_0}(h_T)} + \int_0^{t_0} \Delta \mathcal{C}_{s'}(h_t) dt + \int_{t_0}^T \Delta \mathcal{C}_s(h_t) dt.$$

With usual continuity arguments, we get $\log \rho_{t_0}(h_T) = \log \rho_0(\hat{h}_{T-t_0}) + \int_0^{t_0} \Delta \mathcal{C}_{s'}(\hat{h}_{T-t_0+t}) dt$, where \hat{h}_t is the solution of $\partial_t \hat{h}_t = -\nabla \mathcal{C}_{s'}(\hat{h}_t)$ satisfying $\hat{h}_T = h_T$. Hence,

$$\log \frac{\rho_T(h_T)}{\rho_{t_0}(h_T)} = \log \frac{\rho_0(h_0)}{\rho_0(\hat{h}_{T-t_0})} + \int_0^{t_0} (\Delta \mathcal{C}_{s'}(h_t) - \Delta \mathcal{C}_{s'}(\hat{h}_{T-t_0+t})) dt + \int_{t_0}^T \Delta \mathcal{C}_s(h_t) dt. \quad (8)$$

3. For $\partial_t h_t = -\nabla \mathcal{C}_s(h_t)$ the single-step error is of order $O(\varepsilon^2)$.

Plugging this expression in Proposition 1 we readily obtain a bound whose prior ρ_{t_0} is data-dependent. We refer to Appendix D for an explicit statement of the bound and a derivation of (8).

As a final remark, it is worth mentioning an alternative, and perhaps simpler, approach to obtain a bound with a data-dependent prior. The idea is that we can use s' to find a good prior from which to sample the initialisation of the network. In practice, one can train the model on s' and find a hypothesis \hat{h} . Then, we can choose as ρ_0 any distribution and centre it on \hat{h} . We sample h_0 from ρ_0 and we proceed as usual. Since now ρ_0 is known, we can directly apply Proposition 3.

6. Exact discretised Hamiltonian dynamics

As already mentioned, a main limitation of the bound of Proposition 3 is that it relies on the continuity of the training dynamics in order to control how ρ_t is changing. To overcome this issue, one can consider an alternative optimisation procedure, which allows to keep track of the density's evolution. To do so, we use a Hamiltonian approach, and hence we introduce N additional variables v , representing the velocities (momenta) of the parameters h . The idea is to exploit the fact that the joint density of the pair (h, v) is conserved under the Hamiltonian flow, a property that is preserved for discrete time-steps by suitable symplectic integrators (Hairer et al., 2006). In order to solve an optimisation problem, we can alternate conservative Hamiltonian steps with dissipative ones, which only involve v and entail an exactly computable change in density.

Let us make things more concrete. For the rest of this section, we denote as ρ_k the joint density of (h_k, v_k) . We consider an increasing differentiable map $\psi : \mathbb{R} \rightarrow \mathbb{R}$, such that $\psi(0) = 0$, and we fix $\varepsilon > 0$. We denote as $\Psi_\varepsilon(v)$ the value at $t = \varepsilon$ of the solution of $\partial_t \tilde{v}_t = -\psi(\tilde{v}_t)$ satisfying $\tilde{v}_0 = v_k$, where with a slight abuse of notation we are here implying that ψ is acting component-wise on $\tilde{v}_t \in \mathbb{R}^N$. From (h_k, v_k) , to evaluate (h_{k+1}, v_{k+1}) we first proceed with a dissipative step:

$$h_{k+1/2} = h_k; \quad v_{k+1/2} = \Psi_\varepsilon(v_k).$$

Since this step involves the exact solution of a continuous-time gradient descent evolution, we can appeal to the usual continuity arguments to show that

$$\log \frac{\rho_{k+1/2}(h_{k+1/2}, v_{k+1/2})}{\rho_k(h_k, v_k)} = \sum_{i=1}^N \log \frac{\psi(v_k^i)}{\psi(v_{k+1/2}^i)}, \quad (9)$$

with v^i denoting the i -th component of v (we refer to Appendix E for more details). After this dissipative step, we apply a symplectic Hamiltonian integrator, such as

$$h_{k+1} = h_{k+1/2} + \varepsilon v_{k+1}; \quad v_{k+1} = v_{k+1/2} - \varepsilon \nabla_h \mathcal{C}_s(h_k).$$

This step conserves the density:

$$\rho_{k+1}(h_{k+1}, v_{k+1}) = \rho_{k+1/2}(h_{k+1/2}, v_{k+1/2}).$$

As a concrete example, we can choose $\psi(v) = \eta|v|^p v$, for $p \geq 0$, where $|\cdot|$ denotes the absolute value computed component-wise. The case $p = 0$ corresponds to the standard conformal damped Hamiltonian dynamics (França et al., 2020), and yields to

$$h_{k+1} = h_k + \varepsilon v_{k+1}; \quad v_{k+1} = e^{-\eta\varepsilon} v_k - \varepsilon \nabla_h \mathcal{C}_s(h_k),$$

with a density that increases exponentially as

$$\log \frac{\rho_{k+1}(h_{k+1}, v_{k+1})}{\rho_k(h_k, v_k)} = N\eta\varepsilon.$$

Note that this last term goes linearly with the dimension of the hypothesis space, a behaviour that is likely to bring poor bounds in over-parameterised settings. To avoid this, we choose $p > 0$ and get

$$h_{k+1} = h_k + \varepsilon v_{k+1}; \quad v_{k+1} = \frac{v_k}{(1 + p\eta\varepsilon|v_k|^p)^{1/p}} - \varepsilon \nabla_h \mathcal{C}_s(h_k),$$

and

$$\log \frac{\rho_{k+1}(h_{k+1}, v_{k+1})}{\log \rho_k(h_k, v_k)} = \left(1 + \frac{1}{p}\right) \sum_{i=1}^N \log(1 + p\eta\varepsilon|v_k^i|^p).$$

However, a few empirical tries seem to suggest that also for $p > 0$ the bound brought by these Hamiltonian dynamics is quite loose, even in situations in which the gradient descent dynamics would bring a non-vacuous result. We refer to Appendix E for a few further comments, and defer as future work a more thorough analysis of the problem.

7. Linear models

To give an idea of the behaviour of the bound of Proposition 3, we report here some analytic and empirical results. We consider models linear in the parameters, in the form

$$F_h^i(x) = \sum_j h^{ij} \Phi^j(x),$$

where the Φ^j are some fixed mappings $\mathbb{R} \rightarrow \mathbb{R}$. For binary classification tasks ($y \in \{-1, +1\}$) we let F_h be a real function, and the model's prediction f_h corresponds to the sign of F_h . Conversely, for general multi-class problems the predicted label f_h is the index of the largest component of F_h .

We let ℓ be the 01-loss⁴, so that \mathcal{L}_s and $\mathcal{L}_\mathcal{X}$ represent the empirical and population error. Unless otherwise stated, we will always assume $\mathcal{C}_s(h) = \hat{\mathcal{L}}_s(h) = \frac{1}{m} \sum_{x \in s} \hat{\ell}(F_h(x), f^*(x))$, with $\hat{\ell}$ denoting some twice differentiable surrogate loss function. Applying the chain rule to $\hat{\ell}$, we find

$$\Delta \hat{\ell} = \sum_i \frac{\partial \hat{\ell}}{\partial F^i} \Delta F^i + \sum_{ii'} \frac{\partial^2 \hat{\ell}}{\partial F^i \partial F^{i'}} \nabla F^i \cdot \nabla F^{i'},$$

where Δ and ∇ always refer to derivatives with respect to h . For the linear models that we are considering $\Delta F = 0$ and $\nabla F^i \cdot \nabla F^{i'} = \delta_{ii'} \|\Phi\|^2$. Defining $\Delta_F \hat{\ell} = \sum_i \partial_{F^i}^2 \hat{\ell}$, we get

$$\Delta \hat{\ell} = \|\Phi\|^2 \Delta_F \hat{\ell}. \tag{10}$$

7.1. Linear loss

A first simple example that we can solve analytically is a binary classification problem with

$$\hat{\ell}(F, y) = -Fy.$$

4. $\ell(y, y') = 0$ if $y = y'$; 1 otherwise.

The surrogate loss is linear in F , and so (10) yields $\Delta\hat{\ell} = 0$. In particular, the Laplacian's integral in our bounds vanishes. We can easily solve the evolution dynamics and find that $h_T = h_0 + \gamma T$, where, recalling that $f^*(x)$ is the correct label for x , we have defined $\gamma = \frac{1}{m} \sum_{x \in s} f^*(x) \Phi(x)$. Assuming that under ρ_0 the components of h are all independent centred Gaussians, with variance $1/N$ (N being the dimension of h), we find that $\log \frac{\rho_0(h_0)}{\rho_0(h_T)} = \frac{N}{2} (\|h_T\|^2 - \|h_0\|^2)$. So, (2) becomes

$$\mathcal{L}_{\mathcal{X}}(h_T) - \mathcal{L}_s(h_T) \leq \sqrt{\frac{N}{4m} (2Th_0 \cdot \gamma + T^2 \|\gamma\|^2)} + \frac{1}{2m} \log \frac{2\sqrt{m}}{\delta}.$$

Typically, $\|h_0\| \sim O(1)$, and we expect $\|h_T\| \sim T\|\gamma\|$ to dominate the dynamics. Differently from the $O(\sqrt{T})$ behaviour that we had encountered in section 5.2, now the bound scales linearly with T . Indeed, here h is not approaching a local optimum, but diverging at constant speed γ .

We refer to Appendix F.1 for experiments on linear models trained with the linear surrogate loss.

7.2. Quadratic loss

Another natural situation to solve things explicitly is the case of a quadratic surrogate loss

$$\hat{\ell}(F, y) = \frac{1}{2} (F - \beta y)^2.$$

Here, β is some fixed positive value, and we are still considering a binary classification problem, where the true labels are $+1$ or -1 and the network's prediction is the sign of F . Now, $\Delta_F \hat{\ell} = 1$ and hence (10) yields $\Delta\hat{\ell} = \|\Phi\|^2$. We consider a training objective in the form

$$\mathcal{C}_s(h) = \frac{\alpha \|h\|^2}{2N} + \frac{1}{m} \sum_{x \in s} \hat{\ell}(F_h(x), f^*(x)),$$

with $\alpha \geq 0$ and N the dimension of h . The term $\alpha \|h\|^2 / (2N)$ is introduced to computationally stabilise the algorithm.⁵ We easily find $\int_0^T \Delta \mathcal{C}_s(h_t) dt = \Gamma T$, with $\Gamma = \alpha + \frac{1}{m} \sum_{x \in s} \|\Phi(x)\|^2$. The training dynamics are now governed by $\partial_t h_t = \beta \gamma - \Theta h_t$, where again we have defined $\gamma = \frac{1}{m} \sum_{x \in s} f^*(x) \Phi(x)$, while $\Theta = \frac{\alpha}{N} \text{Id} + \frac{1}{m} \sum_{x \in s} \Phi(x) \Phi(x)^\top$ is a $N \times N$ matrix. For $\alpha > 0$, Θ is invertible and $h_T = h_0 + (\text{Id} - e^{-T\Theta}) (\Theta^{-1} \beta \gamma - h_0)$. For a Gaussian initialisation, (2) becomes

$$\mathcal{L}_{\mathcal{X}}(h_T) - \mathcal{L}_s(h_T) \leq \sqrt{\frac{\frac{N}{2} (\|h_0\|^2 - \|h_T\|^2) + \Gamma T}{2m}}.$$

As the objective is quadratic, for large T this bound behaves as $O(\sqrt{T})$, as it happens more generally when the algorithm is converging to a local quadratic minimum of the objective (see Section 5.2).

We refer to Appendix F.2 for empirical results with the quadratic surrogate loss.

5. In the unregularised case $\alpha = 0$, the matrix inversion Θ^{-1} , necessary to compute h_T , can be source of significant computational errors. Introducing a factor $\alpha > 0$ makes the algorithm more stable.

7.3. Cross-entropy loss

The cross-entropy loss

$$\hat{\ell}(F, y) = \log \left(\sum_i e^{F^i} \right) - F^y$$

is a commonly used objective for multi-class tasks, when $f_h = \operatorname{argmax}_i F_h^i$. In this case we do not have simple analytic dynamics, and we will need to rely on some numerical solution. We have

$$\partial_t h_t^{ij} = -\frac{1}{m} \sum_{x \in \mathcal{S}} \left(\frac{e^{(h_t \Phi(x))^i}}{\sum_k e^{(h_t \Phi(x))^k}} - \delta^{if^*(x)} \right) \Phi^j(x),$$

where $\delta^{if^*(x)}$ denotes the Kronecker delta between the labels i and $f^*(x)$, and

$$\Delta \hat{\ell} = \|\Phi\|^2 \left(1 - \frac{\sum_k e^{2F^k}}{(\sum_k e^{F^k})^2} \right).$$

Contrarily to what happens with the quadratic and linear losses, the objective’s Laplacian is not constant during the training, but tends to decrease. Indeed, for $\hat{\ell}(F, y)$ to be small, we need F^y to be much larger than the other components of F , so that $\sum_k e^{F^k} \simeq e^{F^y}$. This translates into a small Laplacian, as $(\sum_k e^{2F^k})/(\sum_k e^{F^k})^2 \simeq 1$, and we expect the Laplacian’s integral to be asymptotically sublinear in T . Indeed, h_t slowly diverges towards flatter and flatter regions of \mathcal{H} .

We trained linear models of different sizes on MNIST (Deng, 2012), using the cross-entropy loss as objective. Since the dynamics do not admit a simple analytic solution, we performed the classical gradient descent algorithm on batches of the training dataset, with finite time-steps. As discussed in Section 5.4, in this way we do not obtain rigorous generalisation bounds, as we are not following the continuous dynamics. However, we believe that the result that we get are a good approximation of the ones that one would obtain with solving exactly the gradient flow (see Figure 2 and the discussion in Section 5.4). The feature mapping Φ that we used was the composition of a ReLU function and a linear transformation $x \mapsto Wx$, where the components of W were independently sampled from a normal distribution, with variance $1/784$ (784 being the input dimension). We refer to Appendix F.3 for further details.

Table 1 compares the bound (3) with the test error evaluated on a held-out dataset, for different dimensions of the hypothesis space \mathcal{H} , and always with $\delta = 5 \times 10^{-3}$. We chose the best bound among those obtained with 25 different values of T , at the price of adding a penalty factor $\log 25$ (see Section 5.2).

We already stressed in Figure 1 (referring to the same experiment) that the bounds are not negatively affected by the high over-parameterisation, essentially because the optimal time horizon T decreases roughly as $1/N$. The tightest bound was achieved for $N = 10^5$.

Notice that the bounds in Table 1 are comparable to those reported by Clerico et al. (2021) for a stochastic single-hidden-layer network.⁶ Notably, the results therein were obtained using a PAC-Bayesian bound as optimisation objective, while here we are directly optimising the empirical cross-entropy loss, without any regularisation term.

Table 1: Bounds on MNIST

Dimension N	Bound (3)	Test Error
10^3	.3251	.2049
3×10^3	.3034	.1967
10^4	.2786	.1680
3×10^4	.2795	.1541
10^5	.2751	.1602
3×10^5	.2812	.1534
10^6	.2757	.1568

6. Note that Clerico et al. (2021) did not focus on linear models, as both the hidden and outer layers were trained.

8. Conclusion

We established disintegrated PAC-Bayesian bounds for deterministic algorithms, holding with high probability on the random training dataset and initialisation. We tested our findings empirically on linear models, obtaining promising results that are non-vacuous even for highly over-parameterised settings. It is worth mentioning that most empirical PAC-Bayesian results in the literature are derived by using a PAC-Bayesian bound as the optimisation objective (see *e.g.*, [Dziugaite and Roy, 2017](#); [Clerico et al., 2021, 2022a](#); [Pérez-Ortiz et al., 2021a](#); [Zantedeschi et al., 2021](#); [Biggs and Guedj, 2022a](#); [Chérif-Abdellatif et al., 2022](#)), while our bounds directly apply to the standard (continuous-time) empirical risk optimisation. Yet, our bounds on MNIST closely match those obtained by [Clerico et al. \(2021\)](#) on a shallow stochastic network. We defer to future work a more extensive empirical analysis, focusing on data-dependent priors and non-linear models.

A main limitation of our framework is the necessity of continuous-time dynamics. However, it might be possible to obtain rigorous results for the standard discretised gradient descent optimisation via a careful analysis of the numerical error. Alternatively, exact bounds for discrete-time dynamics are available when using suitable damped Hamiltonian integrators. We believe that further investigation in this direction may yield interesting new insights.

Finally, we mention as possible further developments a deeper study of stochastic training dynamics (with the gradient flow’s continuity relation replaced by the Fokker-Planck equation), the case of a training objective depending on the bound itself, and the analysis of the infinite-width limit, where the NTK dynamics ([Jacot et al., 2018](#)) might provide continuous-time exact results.

Acknowledgments

Eugenio Clerico is partially supported by the UK Engineering and Physical Sciences Research Council (EPSRC) through the grant EP/R513295/1 (DTP scheme) and Arnaud Doucet by EPSRC CoSiNES EP/R034710/1. Benjamin Guedj and Arnaud Doucet acknowledge support of the UK Defence Science and Technology Laboratory (DSTL) and EPSRC grant EP/R013616/1. This is part of the collaboration between US DOD, UK MOD and UK EPSRC under the Multidisciplinary University Research Initiative. Benjamin Guedj acknowledges partial support from the French National Agency for Research, grants ANR-18-CE40-0016-01 and ANR-18-CE23-0015-02. The authors would like to thank Umut Şimşekli, Tyler Farghly, and Patrick Rebeschini for the valuable comments and suggestions.

References

- P. Alquier. User-friendly introduction to PAC-Bayes bounds. *arXiv:2110.11216*, 2021.
- P. Alquier and G. Biau. Sparse single-index model. *Journal of Machine Learning Research*, 14(1), 2013.
- A. Banerjee, T. Chen, and Y. Zhou. De-randomized PAC-Bayes margin bounds: Applications to non-convex and non-smooth predictors. *arXiv:2002.09956*, 2020.
- D.G.T. Barrett and B. Dherin. Implicit gradient regularization. *ICLR*, 2021.
- F. Biggs and B. Guedj. Differentiable PAC-Bayes objectives with partially aggregated neural networks. *Entropy*, 23(10), 2021.
- F. Biggs and B. Guedj. On margins and derandomisation in PAC-Bayes. *AISTATS*, 2022a.
- F. Biggs and B. Guedj. Non-vacuous generalisation bounds for shallow neural networks. *ICML*, 2022b.
- G. Blanchard and F. Fleuret. Occam’s hammer. *COLT*, 2007.
- O. Bousquet and A. Elisseeff. Stability and generalization. *Journal of Machine Learning Research*, 2, 2002.
- O. Bousquet, S. Boucheron, and G. Lugosi. *Introduction to Statistical Learning Theory*. Springer, 2004.
- L. Bégin, P. Germain, F. Laviolette, and J.F. Roy. PAC-Bayesian bounds based on the Rényi divergence. *AISTATS*, 2016.
- O. Catoni. *Statistical learning theory and stochastic optimization. Ecole d’été de probabilités de Saint-Flour XXXI-2001*. Springer, 2004.
- O. Catoni. PAC-Bayesian supervised classification: The thermodynamics of statistical learning. *IMS Lecture Notes Monograph Series*, 2007.
- R.T.Q. Chen, Y. Rubanova, J. Bettencourt, and D.K. Duvenaud. Neural ordinary differential equations. *NeurIPS*, 2018.
- B.E. Chérif-Abdellatif, Y. Shi, A. Doucet, and B. Guedj. On PAC-Bayesian reconstruction guarantees for VAEs. *AISTATS*, 2022.
- E. Clerico, G. Deligiannidis, and A. Doucet. Wide stochastic networks: Gaussian limit and PAC-Bayesian training. *arxiv:2106.09798*, 2021.
- E. Clerico, G. Deligiannidis, and A. Doucet. Conditionally Gaussian PAC-Bayes. *AISTATS*, 2022a.
- E. Clerico, A. Shidani, G. Deligiannidis, and A. Doucet. Chained generalisation bounds. *COLT*, 2022b.

- L. Deng. The MNIST database of handwritten digit images for machine learning research. *IEEE Signal Processing Magazine*, 29(6), 2012.
- L. Dinh, R. Pascanu, S. Bengio, and Y. Bengio. Sharp minima can generalize for deep nets. *ICML*, 2017.
- C. Dwork and A. Roth. The algorithmic foundations of differential privacy. *Foundations and Trends in Theoretical Computer Science*, 9, 2014.
- G.K. Dziugaite and D. M. Roy. Computing nonvacuous generalization bounds for deep (stochastic) neural networks with many more parameters than training data. *UAI*, 2017.
- G. França, J. Sulam, D. Robinson, and R. Vidal. Conformal symplectic and relativistic optimization. *NeurIPS*, 2020.
- P. Germain, A. Lacasse, F. Laviolette, and M. Marchand. PAC-Bayesian learning of linear classifiers. *ICML*, 2009.
- B. Ghorbani, S. Krishnan, and Y. Xiao. An investigation into neural net optimization via Hessian eigenvalue density. *ICML*, 2019.
- I. Goodfellow, Y. Bengio, and A. Courville. *Deep Learning*. MIT Press, 2016.
- B. Guedj. A primer on PAC-Bayesian learning. *Proceedings of the Second Congress of the French Mathematical Society*, 2019.
- B. Guedj and P. Alquier. PAC-Bayesian estimation and prediction in sparse additive models. *Electronic Journal of Statistics*, 7, 2013.
- E. Hairer, C. Lubich, and G. Wanner. *Geometric numerical integration*. Springer-Verlag, 2006.
- M. Hardt, B. Recht, and Y. Singer. Train faster, generalize better: Stability of stochastic gradient descent. *ICML*, 2016.
- H. He, G. Huang, and Y. Yuan. Asymmetric valleys: Beyond sharp and flat local minima. *NeurIPS*, 2019.
- K. He, X. Zhang, S. Ren, and J. Sun. Delving deep into rectifiers: Surpassing human-level performance on imagenet classification. *ICCV*, 2015.
- S. Hochreiter and J. Schmidhuber. Flat minima. *Neural Computation*, 9, 1997.
- P. Izmailov, D. Podoprikin, T. Garipov, D. Vetrov, and A.G. Wilson. Averaging weights leads to wider optima and better generalization. *UAI*, 2018.
- A. Jacot, F. Gabriel, and C. Hongler. Neural tangent kernel: Convergence and generalization in neural networks. *NeurIPS*, 2018.
- N.S. Keskar, D. Mudigere, J. Nocedal, M. Smelyanskiy, and P.T.P. Tang. On large-batch training for deep learning: Generalization gap and sharp minima. *ICLR*, 2017.
- J. Langford and M. Seeger. Bounds for averaging classifiers. *CMU technical report*, 2001.

- J. Langford and J. Shawe-Taylor. PAC-Bayes & margins. *NeurIPS*, 2002.
- G. Letarte, P. Germain, B. Guedj, and F. Laviolette. Dichotomize and generalize: PAC-Bayesian binary activated deep neural networks. *NeurIPS*, 2019.
- G. Lugosi and G. Neu. Generalization bounds via convex analysis. *COLT*, 2022.
- A. Maurer. A note on the PAC Bayesian theorem. *arXiv:0411099*, 2004.
- D.A. McAllester. Some PAC-Bayesian theorems. *COLT*, 1998.
- D.A. McAllester. PAC-Bayesian model averaging. *COLT*, 1999.
- K. Miyaguchi. PAC-Bayesian transportation bound. *arXiv:1905.13435*, 2019.
- V. Nagarajan and J.Z. Kolter. Deterministic PAC-Bayesian generalization bounds for deep networks via generalizing noise-resilience. *ICLR*, 2019.
- G. Neu, G.K. Dziugaite, M. Haghifam, and D. M. Roy. Information-theoretic generalization bounds for stochastic gradient descent. *COLT*, 2021.
- B. Neyshabur, S. Bhojanapalli, D.A. McAllester, and N. Srebro. Exploring generalization in deep learning. *NeurIPS*, 2017.
- B. Neyshabur, S. Bhojanapalli, and N. Srebro. A PAC-Bayesian approach to spectrally-normalized margin bounds for neural networks. *ICLR*, 2018.
- M. Pérez-Ortiz, O. Risvaplatá, J. Shawe-Taylor, and C. Szepesvári. Tighter risk certificates for neural networks. *Journal of Machine Learning Research*, 22, 2021a.
- M. Pérez-Ortiz, O. Rivasplata, B. Guedj, M. Gleeson, J. Zhang, J. Shawe-Taylor, M. Bober, and J. Kittler. Learning PAC-Bayes priors for probabilistic neural networks. *arXiv:2109.10304*, 2021b.
- O. Rivasplata, I. Kuzborskij, C. Szepesvári, and J. Shawe-Taylor. PAC-Bayes analysis beyond the usual bounds. *NeurIPS*, 2020.
- L. Sagun, U. Evci, V.U. Güney, Y. Dauphin, and L. Bottou. Empirical analysis of the Hessian of over-parametrized neural networks. *ICLR Workshop*, 2018.
- M. Seeger. PAC-Bayesian generalisation error bounds for Gaussian process classification. *Journal of Machine Learning Research*, 3, 2002.
- S. Shalev-Shwartz and S. Ben-David. *Understanding Machine Learning - From Theory to Algorithms*. Cambridge University Press, 2014.
- Y. Song, J. Sohl-Dickstein, D.P. Kingma, A. Kumar, S. Ermon, and B. Poole. Score-based generative modeling through stochastic differential equations. *ICLR*, 2021.
- V.N. Vapnik. *The Nature of Statistical Learning Theory*. Springer, 2000.

- P. Viallard, P. Germain, A. Habrard, and E. Morvant. A general framework for the disintegration of PAC-Bayesian bounds. *arXiv:2102.08649*, 2021.
- A. Xu and M. Raginsky. Information-theoretic analysis of generalization capability of learning algorithms. *NeurIPS*, 2017.
- V. Zantedeschi, P. Viallard, E. Morvant, R. Emonet, A. Habrard, P. Germain, and B. Guedj. Learning stochastic majority votes by minimizing a PAC-Bayes generalization bound. *NeurIPS*, 2021.
- C. Zhang, S. Bengio, M. Hardt, B. Recht, and O. Vinyals. Understanding deep learning requires rethinking generalization. *Communications of the ACM*, 64, 11 2016.
- W. Zhou, V. Veitch, M. Austern, R.P. Adams, and P. Orbanz. Non-vacuous generalization bounds at the ImageNet scale: a PAC-Bayesian compression approach. *ICLR*, 2019.

Appendix A. Langevin dynamics

We briefly discuss what happens if we try to use Langevin dynamics for the training, that is

$$dh_t = -\nabla \mathcal{C}_s(h_t) dt + \sigma dB_t. \quad (11)$$

Here, $\sigma > 0$ is a diffusion coefficient and B_t denotes the standard Brownian motion. Note that the introduction of noise prevents the bound from diverging at large T if \mathcal{C}_s is bounded from below. Indeed, under suitable regularity conditions for \mathcal{C}_s , ρ_t will converge to the Gibbs equilibrium distribution

$$\rho_\infty(h) = \frac{1}{Z} e^{-2\mathcal{C}_s(h)/\sigma^2},$$

with $Z = \int_{\mathcal{H}} e^{-2\mathcal{C}_s(h)/\sigma^2} dh$ the normalising constant. Letting $M = \sup_{\mathcal{H}} e^{-2\mathcal{C}_s/\sigma^2} < \infty$, ρ_∞ is bounded by M/Z . Asymptotically $\log \frac{\rho_T(h_T)}{\rho_0(h_T)} \lesssim -\log(Z\rho_0(h_T))$, and the bound does not diverge.

For (11), the Fokker-Planck equation yields

$$\partial_t \rho_t(h) = \nabla(\rho_t(h) \nabla \mathcal{C}_s(h)) + \frac{\sigma^2}{2} \Delta \rho_t(h) = \nabla \rho_t(h) \cdot \nabla \mathcal{C}_s(h) + \rho_t(h) \Delta \mathcal{C}_s(h) + \frac{\sigma^2}{2} \Delta \rho_t(h). \quad (12)$$

Applying Itô's lemma we get

$$d(\rho_t(h_t)) = (\rho_t(h_t) \Delta \mathcal{C}_s(h_t) + \sigma^2 \Delta \rho_t(h_t)) dt + \sigma \nabla \rho_t(h_t) \cdot dB_t.$$

Now, writing $u_t = \log \rho_t$, we have

$$du_t(h_t) = \left(\Delta \mathcal{C}_s(h_t) + \frac{\sigma^2}{2} \|\nabla u_t(h_t)\|^2 + \sigma^2 \Delta u_t(h_t) \right) dt + \sigma \nabla u_t(h_t) \cdot dB_t, \quad (13)$$

where we used $\frac{\Delta \rho_t}{\rho_t} = \|\nabla u_t\|^2 + \Delta u_t$. This expression cannot easily be integrated in t , since now we have a dependence on u_t (and hence on ρ_t) in the RHS. In order to obtain a computable bound, one would probably need to upper-bound the intractable quantities in the RHS, an approach that we defer to future work.

An alternative way to tackle the stochastic dynamics consists in converting the SDE (11) in an ODE inducing the same marginal distributions (an idea exploited in [Song et al. \(2021\)](#) in the context of generative modelling). In fact, consider the deterministic flow

$$\partial_t \hat{h}_t = -\nabla \left(\mathcal{C}_s(\hat{h}_t) + \frac{\sigma^2}{2} \log \hat{\rho}_t(\hat{h}_t) \right), \quad (14)$$

where we denote as $\hat{\rho}_t$ the density of \hat{h}_t and we impose $\hat{\rho}_0 = \rho_0$. The continuity equation now reads

$$\partial_t \hat{\rho}_t(h) = \nabla \cdot \left(\hat{\rho}_t(h) \nabla \left(\mathcal{C}_s(h) + \frac{\sigma^2}{2} \log \hat{\rho}_t(h) \right) \right) = \nabla(\hat{\rho}_t(h) \nabla \mathcal{C}_s(h)) + \frac{\sigma^2}{2} \Delta \hat{\rho}_t(h). \quad (15)$$

Comparing (15) with (12), we immediately see that ρ_t and $\hat{\rho}_t$ undergo the same dynamics and, since $\rho_0 = \hat{\rho}_0$, we have that $\rho_t = \hat{\rho}_t$ for all t . In practice, this means that we have two equivalent ways to get $h_T \sim \rho_T$: given an initial point from ρ_0 , we can follow either the stochastic dynamics (11), or the deterministic ones (14), up to time T . Moreover, in order to evaluate the factor $\log \rho_T(h_T)$,

needed for our PAC-Bayesian bound, instead of using (13) we can leverage the continuity equation of the deterministic flow to derive

$$\log \rho_T(h_T) = \log \rho_0(\hat{h}_0) + \int_0^T \Delta \left(\mathcal{C}_s(\hat{h}_t) + \frac{\sigma^2}{2} \log \rho_t(\hat{h}_t) \right) dt,$$

where \hat{h}_t denotes the solution of (14) satisfying $\hat{h}_T = h_T$. Although this expression looks easier than (13), its actual computation is typically unfeasible in practice, due to the RHS's dependence on $\log \rho_t$ (both explicit and implicit, through \hat{h}_t). In the generative modelling context, score matching and neural networks techniques are used to approximate $\nabla \log \rho_t$, but this introduces approximation errors difficult to quantify (Song et al., 2021).

As a final remark, we mention that the dynamics (14) also appear when trying to build an algorithm that directly optimises a PAC-Bayesian bound. Indeed, for $\ell \subseteq [0, 1]$, the choice $\Psi(u, v) = \frac{2}{\sigma^2}(v - u)$ (for an arbitrary $\sigma > 0$) in Proposition 1 leads to a bound in the form

$$\mathcal{L}_{\mathcal{X}}(h_T) \leq \mathcal{L}_s(h_T) + \frac{1}{4m\sigma^2} + \frac{\sigma^2}{2} \left(\log \frac{\rho_T(h_T)}{\rho_0(h_T)} + \log \frac{1}{\delta} \right).$$

Using this bound as optimisation objective is equivalent to follow the dynamics (14), provided that we set $\mathcal{C}_s(h) = \mathcal{L}_s(h) + \frac{1}{4m\sigma^2} + \frac{\sigma^2}{2}(-\log \rho_0(h) + \log \frac{1}{\delta})$. We defer to future work a deeper analysis of this connection.

Appendix B. Rewriting the Laplacian's integral

We explicitly derive here (6). First, notice that $\partial_t \log \|\nabla \mathcal{C}_s(h_t)\| = -\frac{\nabla \mathcal{C}_s(h_t)}{\|\nabla \mathcal{C}_s(h_t)\|} \cdot \nabla \|\nabla \mathcal{C}_s(h_t)\|$. Since, for all h ,

$$\Delta \mathcal{C}_s(h) = \nabla \cdot \nabla \mathcal{C}_s(h) = \nabla \cdot \left(\frac{\nabla \mathcal{C}_s(h)}{\|\nabla \mathcal{C}_s(h)\|} \right) \|\nabla \mathcal{C}_s(h)\| + \frac{\nabla \mathcal{C}_s(h)}{\|\nabla \mathcal{C}_s(h)\|} \cdot \nabla \|\nabla \mathcal{C}_s(h)\|,$$

we get

$$\Delta \mathcal{C}_s(h_t) = \nabla \cdot \left(\frac{\nabla \mathcal{C}_s(h_t)}{\|\nabla \mathcal{C}_s(h_t)\|} \right) \|\nabla \mathcal{C}_s(h_t)\| - \partial_t \log \|\nabla \mathcal{C}_s(h_t)\|.$$

We conclude that

$$\int_0^T \Delta \mathcal{C}_s(h_t) dt = \log \frac{\|\nabla \mathcal{C}_s(h_0)\|}{\|\nabla \mathcal{C}_s(h_T)\|} + \int_0^T \nabla \cdot \left(\frac{\nabla \mathcal{C}_s(h_t)}{\|\nabla \mathcal{C}_s(h_t)\|} \right) \|\nabla \mathcal{C}_s(h_t)\| dt.$$

The integral in the RHS is a line-integral along the path $h_{[0,T]}$, as $\|\nabla \mathcal{C}_s(h)\|$ is the norm of the flow's "velocity" in h . Moreover, $\tau(h) = -\frac{\nabla \mathcal{C}_s(h)}{\|\nabla \mathcal{C}_s(h)\|}$ is the unit tangent vector to the gradient flow in h . We can thus write

$$\int_0^T \Delta \mathcal{C}_s(h_t) dt = \log \frac{\|\nabla \mathcal{C}_s(h_0)\|}{\|\nabla \mathcal{C}_s(h_T)\|} - \int_{h_{[0,T]}} \nabla \cdot \tau(h) \|\delta h\|,$$

which is (6).

Appendix C. Asymptotic behaviour around a local minimum

We consider the case in which the algorithm is approaching a quadratic local optimum of \mathcal{C}_s . We will hence say that for t larger than some \hat{t} we have

$$\mathcal{C}_s(h_t) \simeq \mathcal{C}_s(h^*) + \frac{1}{2}(h_t - h^*)^\top H(h_t - h^*),$$

where H is a positive definite matrix, namely the Hessian of \mathcal{C}_s evaluated at h^* . Hence, for $t \geq \hat{t}$ the objective's Laplacian is roughly constant,

$$\Delta\mathcal{C}_s(h_t) \simeq \text{Tr}[H].$$

For a large enough time horizon T , we can asymptotically write $\int_0^T \Delta\mathcal{C}_s(h_t) \simeq T\text{Tr}[H]$. Moreover, since the Laplacian's integral is diverging while $\frac{\rho_0(h_0)}{\rho_0(h_T)} \rightarrow \frac{\rho_0(h^*)}{\rho_0(h_T)}$, asymptotically we find that (2) takes the form

$$\mathcal{L}_{\mathcal{X}}(h_T) - \mathcal{L}_s(h_T) \lesssim O\left(\sqrt{\frac{T\text{Tr}[H]}{2m}}\right).$$

Appendix D. Data-dependent priors

As we discussed in Section 5.6, if we want to use a prior ρ_{t_0} , learnt on a dataset s' (independent of s), we need to evaluate $\log \rho_{t_0}(h_T)$. Define \hat{h}_t as the solution of $\partial_t \hat{h}_t = -\nabla\mathcal{C}_{s'}(\hat{h}_t)$ satisfying $\hat{h}_T = h_T$. We have that

$$\log \rho_{t_0}(h_T) = \log \rho_{t_0}(\hat{h}_T) = \log \rho_0(\hat{h}_{T-t_0}) + \int_0^{t_0} \partial_t (\log \rho_t(\hat{h}_{T-t_0+t})) dt.$$

Since, for $t \in [0, t_0]$, ρ_t is the push-forward of ρ_0 under the gradient dynamics with objective $\mathcal{C}_{s'}$, we have that for all h

$$\partial_t \rho_t(h) = \rho_t(h) \Delta\mathcal{C}_{s'}(h) + \nabla \rho_t(h) \cdot \nabla \mathcal{C}_{s'}(h)$$

and so in particular

$$\partial_t (\rho_t(\hat{h}_t)) = \partial_t \rho_t(\hat{h}_t) + \nabla \mathcal{C}_{s'}(\hat{h}_t) \cdot \partial_t \hat{h}_t = \rho_t(\hat{h}_t) \Delta\mathcal{C}_{s'}(\hat{h}_t).$$

We conclude that

$$\log \rho_{t_0}(h_T) = \log \rho_0(\hat{h}_{T-t_0}) + \int_0^{t_0} \Delta\mathcal{C}_{s'}(\hat{h}_{T-t_0+t}) dt,$$

from which (8) follows. We can hence state the following variant of Proposition 3 for data-dependent priors.

Proposition 4 *Let s and s' be independent training dataset, with $s \sim \mu^m$. Let \mathcal{C}_s and $\mathcal{C}_{s'}$ be two twice differentiable training objectives, fix $T > 0$ and $t_0 \in [0, T)$. Consider an algorithm that, for an initial state h_0 , follows the dynamics $\partial_t h_t = -\nabla\mathcal{C}_{s'}(h_t)$ for $t \in [0, t_0]$, and $\partial_t h_t = -\nabla\mathcal{C}_s(h_t)$*

for $t \in [t_0, T]$, and finally outputs h_T . Then, for any measurable function $\Psi : \mathbb{R}^2 \rightarrow \mathbb{R}$, with probability at least $1 - \delta$ on the random draw $(s, h_0) \sim \mu^m \otimes \rho_0$, we have

$$\begin{aligned} & \Psi(\mathcal{L}_s(h_T), \mathcal{L}_X(h_T)) \\ & \leq \log \frac{\rho_0(h_0)}{\rho_0(\hat{h}_{T-t_0})} + \int_0^{t_0} (\Delta \mathcal{C}_{s'}(h_t) - \Delta \mathcal{C}_{s'}(\hat{h}_{T-t_0+t})) dt + \int_{t_0}^T \Delta \mathcal{C}_s(h_t) dt + \log \frac{\xi}{\delta}, \end{aligned}$$

where $\xi = \int_{\mathcal{X}^m \times \mathcal{H}} e^{\Psi(\mathcal{L}_s(h), \mathcal{L}_X(h))} d\mu^m(s) d\rho_{t_0}(h)$, and \hat{h}_t is the solution of $\partial_t \hat{h}_t = -\nabla \mathcal{C}_{s'}(\hat{h}_t)$ satisfying $\hat{h}_T = h_T$.

Appendix E. Hamiltonian dynamics

In this section we give some further details on the damped Hamiltonian dynamics that we have mentioned in Section 6. First, let us derive the density update due to the dissipative step

$$\begin{aligned} h_{k+1/2} &= h_k; \\ v_{k+1/2} &= \Psi_\varepsilon(v_k). \end{aligned}$$

Recall that $\Psi_\varepsilon(v_k)$ is the solution at time $t = \varepsilon$ of $\partial_t \tilde{v}_t = -\psi(\tilde{v}_t)$, with ψ acting component-wise and $\tilde{v}_0 = v_k$. The continuity equation applied to this gradient flow brings

$$\log \rho_{k+1/2}(h_{k+1/2}, v_{k+1/2}) = \log \rho_k(h_k, v_k) + \int_0^\varepsilon \nabla \cdot \psi(\tilde{v}_t) dt.$$

Now, since ψ is applied to \tilde{v}_t component-wise, we can proceed as we did at the beginning of Section 5.1 when dealing with a one-dimensional optimisation objective, and see that for each component of \tilde{v}_t

$$\psi'(\tilde{v}_t^i) = \frac{\partial_t(\psi(\tilde{v}_t^i))}{\partial_t \tilde{v}_t^i} = -\frac{\partial_t(\psi(\tilde{v}_t^i))}{\psi(\tilde{v}_t^i)} = -\partial_t(\log \psi(\tilde{v}_t^i)),$$

and so

$$\int_0^\varepsilon \psi'(\tilde{v}_t^i) dt = \log \frac{\psi(\tilde{v}_0^i)}{\psi(\tilde{v}_\varepsilon^i)} = \log \frac{\psi(v_k^i)}{\psi(v_{k+1/2}^i)},$$

from which (9) follows.

The Hamiltonian step that comes after is

$$\begin{aligned} h_{k+1} &= h_{k+1/2} + \varepsilon v_{k+1}; \\ v_{k+1} &= v_{k+1/2} - \varepsilon \nabla_h \mathcal{C}_s(h_k), \end{aligned}$$

which means that we are applying to (h_k, v_k) the transformation

$$\begin{pmatrix} h \\ v \end{pmatrix} \mapsto \begin{pmatrix} h + \varepsilon v - \varepsilon^2 \nabla \mathcal{C}_s(h) \\ v - \varepsilon \nabla \mathcal{C}_s(h) \end{pmatrix},$$

whose jacobian $\begin{pmatrix} 1 - \varepsilon^2 \Delta \mathcal{C}_s(h) & \varepsilon \\ -\varepsilon \Delta \mathcal{C}_s(h) & 1 \end{pmatrix}$ has determinant 1 for all h and v . Consequently, this transformation conserve the density, in the sense that $\rho_{k+1}(h_{k+1}, v_{k+1}) = \rho_{k+1/2}(h_{k+1/2}, v_{k+1/2})$.

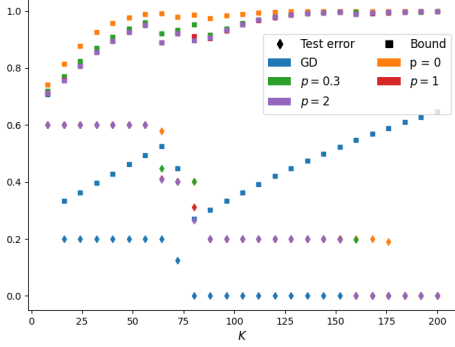


Figure 3: Behaviour of the bound (3) and the test error for different values of K , for a linear model with 5000 parameters, trained to optimise the cross-entropy loss via gradient descent and damped Hamiltonian dynamics (with different choices of the exponent p in ψ). The data came from five different Gaussian distributions on \mathbb{R}^5 that had been assigned five different labels. The training dataset counted 500 datapoints and a held-out test dataset was used to evaluate the test errors reported. The Hamiltonian dynamics always lead to vacuous bounds, and only the gradient descent training was able to bring a non-vacuous result. See Appendix F.4 for further details.

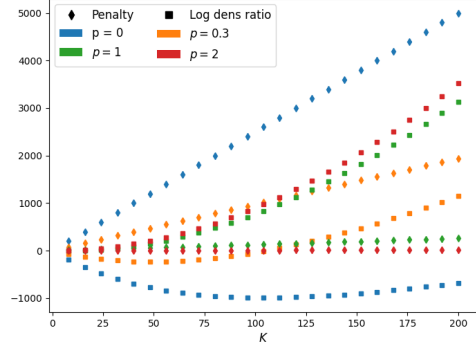


Figure 4: In the same experiment described in Figure 3 (see Appendix F.4 for details), behaviour of the log density ratio $\log \frac{\rho_0(h_0, v_0)}{\rho_0(h_K, v_K)}$ and of the penalty factor $\sum_{k=0}^{K-1} \sum_{i=1}^N \log \frac{\psi(v_k^i)}{\psi(v_{k+1/2}^i)}$, for different values of p and K . Note that increasing p leads to a lower penalty factor, but at the same time to a larger log density ratio.

Following the above dynamics for K steps and applying Proposition 1 leads to the bound

$$\Psi(\mathcal{L}_{\mathcal{X}}(h_K), \mathcal{L}_s(h_K)) \leq \log \frac{\xi}{\delta} + \log \frac{\rho_0(h_0, v_0)}{\rho_0(h_K, v_K)} + \sum_{k=0}^{K-1} \sum_{i=1}^N \log \frac{\psi(v_k^i)}{\psi(v_{k+1/2}^i)}. \quad (16)$$

As usual, Ψ is an arbitrary measurable function $\mathbb{R}^2 \rightarrow \mathbb{R}$, ξ is the expectation of $e^{\Psi(\mathcal{L}_{\mathcal{X}}(h_K), \mathcal{L}_s(h_K))}$ under $\mu^m \otimes \rho_0$, and the bound holds with probability at least $1 - \delta$ on $(s, h_0, v_0) \sim \mu^m \otimes \rho_0$.

Letting $\psi(v) = \eta v$ (for $\eta > 0$) leads to the classical conformal dissipative dynamics (França et al., 2020)

$$\begin{aligned} h_{k+1} &= h_k + \varepsilon v_{k+1}; \\ v_{k+1} &= e^{-\eta \varepsilon} v_k - \varepsilon \nabla \mathcal{C}_s(h_k), \end{aligned}$$

with a change of density given by

$$\log \frac{\rho_{k+1}(h_{k+1}, v_{k+1})}{\rho_k(h_k, v_k)} = \eta \varepsilon N.$$

In particular, the bound's penalty will be $K \eta \varepsilon N$ and hence grow linearly with the dimension of \mathcal{H} . This does not look like a very promising behaviour in order to obtain tight bounds for parameterised

algorithms. Figure 3 shows that indeed even for a simple classification task the bound can end up being pretty loose.

In order to solve this issue, we tried to use a more general form of ψ and set $\psi(v) = \eta|v|^p v$ with $p \geq 0$, where $|\cdot|$ denotes the component-wise absolute value. Clearly, $p = 0$ corresponds to the linear dissipative term that we have just discussed. On the other hand, for $p > 0$ one can easily check that $\Psi_\varepsilon(v) = \frac{v}{(1+p\eta\varepsilon|v|^p)^{1/p}}$. Hence, for each component of v , $\frac{\psi(v_k^i)}{\psi(v_{k+1/2}^i)} = (1 + p\eta\varepsilon|v|^p)^{(1+p)/p}$, which means that

$$\log \frac{\rho_{k+1}(h_{k+1}, v_{k+1/2})}{\log \rho_k(h_k, v_k)} = \left(1 + \frac{1}{p}\right) \sum_{i=1}^N \log (1 + p\eta\varepsilon|v_k^i|^p) .$$

We expect the components of v to be smaller than 1 (at the initialisation typically we will sample them from a Gaussian with small variance) and hence we can hope that the penalty term will now have a better behaviour with N . This is indeed the case for the last term in the RHS of (16). However, the results from figure 4 show that this improvement comes at the price of a larger $\log \frac{\rho_0(h_0, v_0)}{\rho_0(h_K, v_K)}$, due to the fact that less dissipative dynamics allow the model to explore a wider region of the hypothesis space, ending up with a final state (h_K, v_K) with a ρ_0 density much lower than $\rho_0(h_0, v_0)$. Consequently, for the experiment of Figure 3 we were not able to get non-vacuous bounds, even for $p > 0$. On the other hand, the bound obtained with the gradient descent approach was much tighter. We refer to Section F.4 for the experimental details.

It is unclear so far if a better choice of ψ could lead to tight bounds. We leave the investigation of this open problem as future work.

Appendix F. Experimental details

F.1. Linear loss

We tested empirically the behaviour of the bounds (2) and (3) with a linear surrogate loss (see Section 7.1). We used a binary toy dataset, which was created as follows. First, we sampled eight

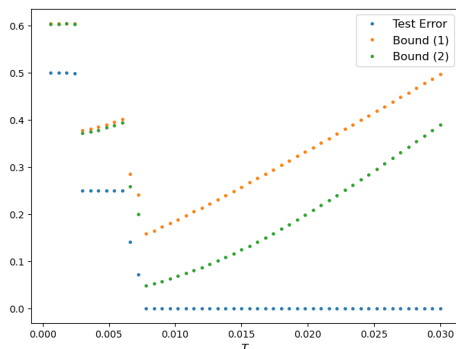


Figure 5: Behaviour of the bounds (2) and (3) for a linear model with 10000 parameters, trained with a linear surrogate loss, for different time horizons.

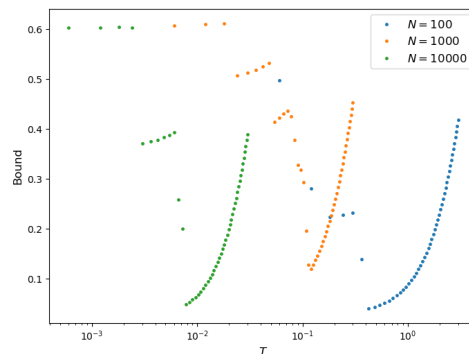


Figure 6: For the experiments with the linear surrogate loss, comparison of the evolution of the bound (3) for different sizes N of the the model.

independent points in \mathbb{R}^5 , from a standard normal distribution. These eight points were then used as the means of eight Gaussian distributions, symmetric and with variance 0.1. We sampled eight Gaussian clusters of 5000 independent points from each of this eight distributions. We then assigned the label -1 to four clusters, and $+1$ to the remaining four. Finally, all the points were projected on the unit sphere. 500 of them, randomly chosen, were used as training dataset, while the remaining 39500 constituted a held-out test dataset.

The linear model that we considered was a neural network with a single hidden layer, where the hidden nodes were kept fixed at their initial values and only the outer layer was trained. Explicitly, we had $F(x) = h \cdot \Phi(x)$, with $\Phi(x) = \phi(Wx)$. Here, W denotes a random $N \times 5$ matrix (whose components were independently drawn from a centred normal distribution with variance $1/5$) and ϕ is the ReLU function $\phi(x) = \max(0, x)$. We chose as ρ_0 a multivariate normal distribution, so that all the components of h_0 were independent draws from a centred Gaussian random variable with variance $1/N$.

We tried different values for the dimension N of h : 100, 1000, and 10000. We report in Figure 5 in the main text the results obtained for $N = 10000$, for 50 possible values of the time horizon T . The parameter δ was fixed at .005, so the bounds hold with probability higher than .995. Since the values reported are already comprehensive of the factor $\log 50$ due to the union bound, it is possible to select the time horizon T yielding the tightest result. Figure 6 compares the values of (3) for the different sizes N .

F.2. Quadratic loss

For the experiments with the quadratic surrogate loss (see Section 7.2), we used the same binary dataset and models that we described in Appendix F.1. The parameters α and β that define \mathcal{C}_s were both set to 1. Figure 7 reports the results obtained for $N = 10000$. The value reported are already taking into account the $\log 50$ factor (due to the union bound), and δ was again chosen to be .005. Figure 8 compares the values of the bound (3) for different dimensions N .

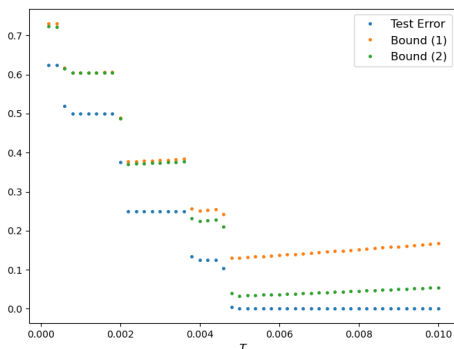


Figure 7: Behaviour of the bounds (2) and (3) for a linear model with 10000 parameters, trained with a quadratic surrogate loss, for different time horizons.

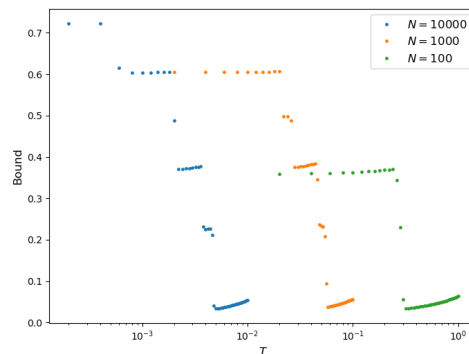


Figure 8: For the experiments with the quadratic surrogate loss, comparison of the evolution of the bound (3) for different sizes N of the the model.

E.3. Cross-entropy loss

We performed our experiments with the cross-entropy as surrogate loss (see Section 7.3) on the MNIST dataset, with the standard split of 60000 images used for the training and 10000 for the testing of the model. The training was performed on batches of 500 elements. The images were flattened to one-dimensional arrays and renormalised. We used again linear architectures $F(x) = h\Phi(x)$, but now with h being a $10 \times w$ matrix (w denoting the width of the network). Φ was always in the form $\Phi(x) = \phi(Wx)$. Here ϕ acts component-wise as the ReLU function, and W is a $w \times 784$ matrix (784 being the dimension of the input datapoints), whose components were independently drawn from a centred normal distribution with variance $1/784$. The dimension of the hypothesis h was $N = 10w$, as the networks had 10 output nodes. We tested different values of N , as reported in Table 1. In all the bounds $\delta = .005$.

Table 2: Time discretisation

Dimension N	Final Time	δ_t
10^3	60	2.00×10^{-2}
3×10^3	20	6.67×10^{-3}
10^4	6	2.00×10^{-3}
3×10^4	2	6.67×10^{-4}
10^5	.6	2.00×10^{-4}
3×10^5	.2	6.67×10^{-5}
10^6	.06	2.00×10^{-5}

Since closed-form solutions for the flow are not available, we used discretised gradient dynamics. For each batch s_k we made an update $h_{t+\delta_t} = h_t + \delta_t \nabla \mathcal{C}_{s_k}(h_t)$, for some small δ_t . Recall that, when training by batches, the Laplacian’s integral takes the form (7). Here we chose that $t_k = k\delta_t$, so that every time we switched to a new batch after a single time-step. In particular, we get $\int_{t_{k-1}}^{t_k} \Delta \mathcal{C}_{s_k}(h_t) dt = \Delta \mathcal{C}_{s_k}(h_{t-1}) \delta_t$ in (7). Table 2 reports the different values of time discretisations δ_t , used for the models that we trained. Figure 2 in the main text shows the relative error between the values of (3) obtained for the same model ($N = 10^5$) for two different time discretisations ($\delta_{t,1} = 2 \times 10^{-4}$ and $\delta_{t,2} = 2 \times 10^{-6}$). In both cases we trained for a time-interval of 2×10^{-4} before switching batch. This means that for $\delta_{t,1}$ each batch was used for a single time-step, before

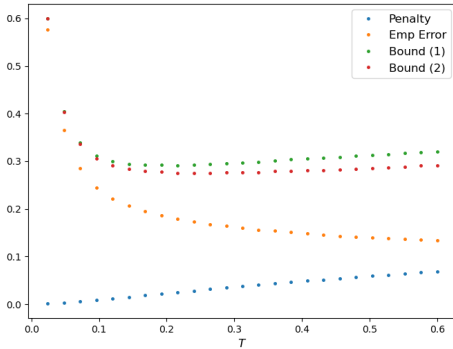


Figure 9: Behaviour of the bounds (2) and (3) at different time horizons T , for a linear model with 10^5 parameters trained with the cross-entropy loss on MNIST. The plot also shows the values of the penalty factor $\frac{1}{m} (\log \frac{\rho_0(h_0)}{\rho_0(h_T)} + \log \frac{25\sqrt{m}}{\delta}) + \int_0^T \Delta \mathcal{C}_s(h_t) dt$, where $\delta = 5 \times 10^{-3}$.

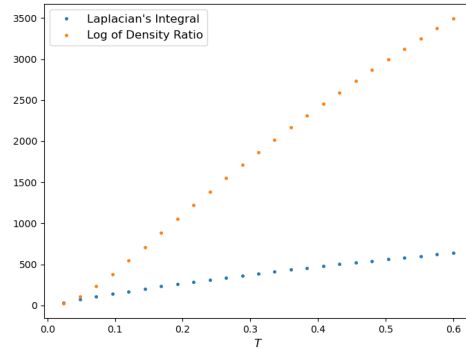


Figure 10: For the same experiment illustrated in Figure 9, comparison of the log density ratio $\log \frac{\rho_0(h_0)}{\rho_0(h_T)}$ and the Laplacian’s integral $\int_0^T \Delta \mathcal{C}_s(h_t) dt / m$. The log density ratio is clearly the dominant term. Note that the contribution of $\log \frac{25\sqrt{m}}{\delta} \simeq 14.02$ to the bound is negligible.

switching to the next one, while for $\delta_{t,2}$ 100 gradient-steps were performed on each batch before passing to the next one.

The values of (3) that we obtained for the different dimensions N are reported in Table 1, in the main text. The penalty $\log 25$ is already taken into account for the values reported, as for each width the best bound has been chosen among the values obtained with 25 different time horizons. The optimal T reported in Figure 1 are the values of the best time horizon (among the 25 ones that we tried) that we obtained for each model’s width. Figures 9 and 10 refer to the model with size $N = 10^5$. Figure 9 shows the evolution of the bounds (2) and (3) during the training. The values of the empirical error and of the penalty factor $(\log \frac{\rho_0(h_0)}{\rho_0(h_T)} + \log \frac{25\sqrt{m}}{\delta} + \int_0^T \Delta \mathcal{C}_s(h_t) dt)/m$ are also reported. Figure 10 compares the contributions of the Laplacian’s integral and the log-density term, showing that here it is the latter that dominates.

F.4. Hamiltonian dynamics

To test the Hamiltonian setting described in Section 6 and Appendix E, we used a linear network with width 1000 and 5 output nodes (so $N = 5000$) on a classification tasks with 5 different labels. The dataset was created as follows. First, we sampled five independent points in \mathbb{R}^5 , from a standard normal distribution. These five points were then used as the means of five Gaussian distributions, symmetric and with variance 0.1. We sampled five Gaussian clusters of 5000 independent points from each of this five distributions. We then assigned the label a different label to each cluster. Finally, all the points were projected on the unit sphere. 500 of them, randomly chosen, were used as training dataset, while the remaining 24500 constituted a held-out test dataset.

The linear model that we considered was a neural network with a single hidden layer, where the hidden nodes were kept fixed at their initial values and only the outer layer was trained. Explicitly, we had $F(x) = h\Phi(x)$, with $\Phi(x) = \phi(Wx)$. Here, W denotes a random 1000×5 matrix (whose components were independently drawn from a centred normal distribution with variance 1/5) and ϕ is the ReLU function $\phi(x) = \max(0, x)$. h was a 5×1000 matrix, whose initial components were independent draws from a centred Gaussian random variable with variance 1/1000.

First we trained the model via (discrete-time) gradient descent, using the cross entropy loss. The time-step chosen was $\delta_t = .005$. We used 25 possible time horizon, and evaluated the bounds for $\delta = .005$. Then, we tested the Hamiltonian dynamics. We sampled the initial v_0 so that its components were whose were independent draws from a centred Gaussian random variable with variance 1/1000. We then trained the same model using different values of p in the definition of ψ . The results obtained can be found in Figures 3 and 4.